AFRL-ML-WP-TR-2003-4013

SILICON CARBIDE SUBSTRATES FOR GaN RESEARCH AND DEVELOPMENT

Marek Skowronski

Carnegie Mellon University
Department of Materials Science and Engineering
5000 Forbes Avenue
Pittsburgh, PA 15213

DECEMBER 2002

Final Report for 29 July 2000 – 30 June 2002

MATERIALS AND MANUFACTURING DIRECTORATE
AIR FORCE RESEARCH LABORATORY
AIR FORCE MATERIEL COMMAND
WRIGHT-PATTERSON AIR FORCE BASE, OH 45433-7750

NOTICE

USING GOVERNMENT DRAWINGS, SPECIFICATIONS, OR OTHER DATA INCLUDED IN THIS DOCUMENT FOR ANY PURPOSE OTHER THAN GOVERNMENT PROCUREMENT DOES NOT IN ANY WAY OBLIGATE THE US GOVERNMENT. THE FACT THAT THE GOVERNMENT FORMULATED OR SUPPLIED THE DRAWINGS, SPECIFICATIONS, OR OTHER DATA DOES NOT LICENSE THE HOLDER OR ANY OTHER PERSON OR CORPORATION; OR CONVEY ANY RIGHTS OR PERMISSION TO MANUFACTURE, USE, OR SELL ANY PATENTED INVENTION THAT MAY RELATE TO THEM.

THIS REPORT IS RELEASABLE TO THE NATIONAL TECHNICAL INFORMATION SERVICE (NTIS). AT NTIS, IT WILL BE AVAILABLE TO THE GENERAL PUBLIC, INCLUDING FOREIGN NATIONS.

THIS TECHNICAL REPORT HAS BEEN REVIEWED AND IS APPROVED FOR PUBLICATION.

WILLIAM C. MITCHEL, Project Engineer
Sensor Materials Branch
Survivability & Sensor Materials Division

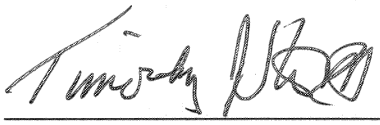

TIMOTHY J. STRANGE, Chief
Sensor Materials Branch
Survivability & Sensor Materials Division

KATHERINE A. STEVENS, Chief
Survivability & Sensor Materials Division
Materials & Manufacturing Directorate

Do not return copies of this report unless contractual obligations or notice on a specific document requires its return.

REPORT DOCUMENTATION PAGE

Form Approved
OMB No. 0704-0188

1. REPORT DATE *(DD-MM-YY)*	2. REPORT TYPE	3. DATES COVERED *(From - To)*
December 2002	Final	07/29/2000 – 06/30/2002

4. TITLE AND SUBTITLE
SILICON CARBIDE SUBSTRATES FOR GaN RESEARCH AND DEVELOPMENT

5a. CONTRACT NUMBER
F33615-00-C-5410

5b. GRANT NUMBER

5c. PROGRAM ELEMENT NUMBER
62102F

6. AUTHOR(S)
Marek Skowronski

5d. PROJECT NUMBER
4348

5e. TASK NUMBER
71

5f. WORK UNIT NUMBER
20

7. PERFORMING ORGANIZATION NAME(S) AND ADDRESS(ES)
Carnegie Mellon University
Department of Materials Science and Engineering
5000 Forbes Avenue
Pittsburgh, PA 15213

8. PERFORMING ORGANIZATION REPORT NUMBER

9. SPONSORING/MONITORING AGENCY NAME(S) AND ADDRESS(ES)
Materials and Manufacturing Directorate
Air Force Research Laboratory
Air Force Materiel Command
Wright-Patterson AFB, OH 45433-7750

10. SPONSORING/MONITORING AGENCY ACRONYM(S)
AFRL/MLPS

11. SPONSORING/MONITORING AGENCY REPORT NUMBER(S)
AFRL-ML-WP-TR-2003-4013

12. DISTRIBUTION/AVAILABILITY STATEMENT
Approved for public release; distribution is unlimited.

13. SUPPLEMENTARY NOTES
Report contains color.

14. ABSTRACT

6H-SiC boules have been grown by physical vapor transport (PVT) method and analyzed using mass spectroscopy (glow discharge and secondary ion) and transport methods. The dominant impurities in crystals grown from commercial SiC charge are nitrogen and boron. Nitrogen concentrations decrease toward the tail while that of boron and aluminum increase. The Fermi level in all crystals started at being pinned to nitrogen donor level in the seed end of the boule and dropped to the shallow boron acceptor level at the tail end. The middle part exhibited either a narrow or wide band of high-resistivity material, depending primarily on the impurity content and segregation. The transition metals have a low incorporation coefficient in 6H-SiC and even in intentionally doped crystals were below mass spectroscopy detection limit.

15. SUBJECT TERMS
6H SiC boules, physical vapor transport method

16. SECURITY CLASSIFICATION OF:			17. LIMITATION OF ABSTRACT:	18. NUMBER OF PAGES	19a. NAME OF RESPONSIBLE PERSON (Monitor)
a. REPORT	b. ABSTRACT	c. THIS PAGE			William C. Mitchel
Unclassified	Unclassified	Unclassified	SAR	36	19b. TELEPHONE NUMBER *(Include Area Code)* (937) 255-4474 x3214

Table of Contents

List of figures

Figure **Page**

List of Tables

Table **Page**

1. Introduction

This research project was focused on the identification of compensation mechanisms in silicon carbide (SiC) single crystals grown by the physical vapor transport (PVT) method and the exploration of intentional doping with transition metal ions. All crystals grown and characterized were of 6H-SiC polytype. Specifically, Carnegie Mellon University addressed the following:

- PVT growth of 6H-SiC crystals.
- Investigation of compensation and deep levels by Hall effect measurements.
- Intentional doping with transition metal ions.
- Segregation of residual and intentional impurities in PVT-grown crystals.

2. PVT Growth of 6H-SiC Crystals.

1.1 System Description.

The schematic diagram of the PVT growth system and the details of the hot zone are shown in Figure 1 (a) and (b). The hot zone was located in a double wall water-cooled quartz chamber with heating provided by a high-frequency field. The system did not have any moving parts, with the exception of the adjustable coil, which was moved up and down by a stepping motor. The chamber walls and hot zone were supported by a stainless steel support ring and graphite cylinder, respectively. In addition, the support ring provided several ports for vacuum gauges, gas inlet, exhaust, and a port for turbomolecular pump. The temperature of the growth crucible was monitored by two two-color pyrometers and two viewports located in the center of the top and bottom plates.

The hot zone was constructed of two grades of graphite: a dense graphite used for the support rod, susceptor, and crucible, and carbon-bonded carbon fiber (CBCF) insulation surrounding the susceptor. The radio frequency (RF) field with a frequency of 10 kHz couples mostly to the graphite susceptor cylinder and does not penetrate into the crucible, charge powder, or growing crystal. The desired temperature gradient was achieved by adjusting the position of the RF coil in respect to the hot zone and by choosing the size of the opening in the top and bottom insulation discs. Radiation escaping through the top opening provided an effective heat extraction mechanism.

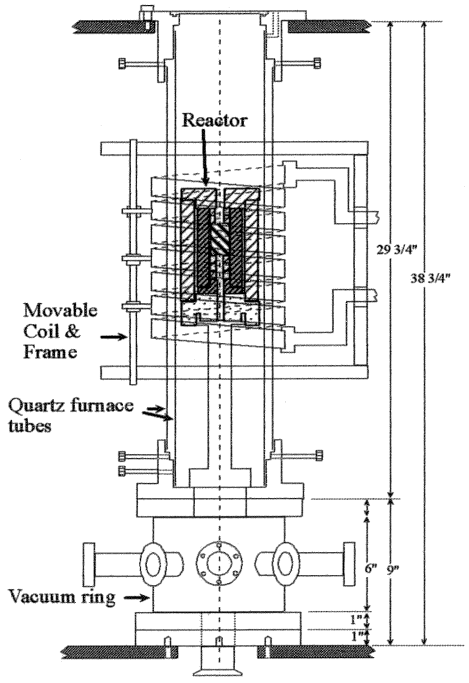

Figure 1. Schematic diagram of the SiC PVT reactor

SiC wafers used as seeds were mounted on the crucible lid using graphitized sucrose. The crystal surface faced down during growth. The solid charge material filled most of the crucible volume. Growth runs were conducted at a temperature of 2200 °C, with a temperature difference between the top and bottom surfaces of the crucible of about 20 °C. All growth runs were performed at the same inert gas pressure of 5 torr. Ultra-high-purity argon (99.999 percent purity) was used for purging and backfilling the chamber. The residual doping based on the purity of the inert gas was below 10^{15} cm^{-3} and could introduce only gaseous impurities such as nitrogen and oxygen in measurable quantities. Nitrogen analysis is discussed in one of the following sections.

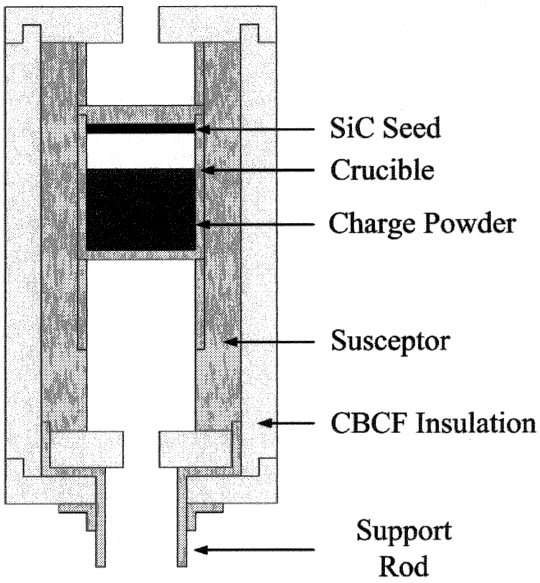

Figure 2. Schematic diagram of the hot zone used in all growth experiments.

Figure Note: Only four types of materials have been used inside the hot zone: dense halogen-purified graphite for the susceptor, crucible, and support; rigid graphite insulation; SiC charge powder; and SiC single-crystal seed.

2.2 Purity of Starting Materials.

All elements of the furnace, except for the hot zone and the support rod, remained cold during the growth runs and are unlikely to have contributed to the residual contamination of the grown crystals. The growth parameters that are of importance from the point of view of residual impurity content and electrical conductivity are growth temperature, purity of charge material and materials used in the construction of the hot zone, stoichiometry and amount of source material, and pregrowth procedures such as length of time, vacuum level, and temperature of pregrowth annealing. The exhaustive study of all of the above parameters is needed in order to fully understand the processes responsible for control of impurity incorporation during PVT growth and their effects on electrical compensation. It was, however, beyond the scope of this project due to time and financial constraints. Instead, Carnegie Mellon University focused on correlation of

materials used in the growth, impurity content in resulting crystals, their electrical resistivity and Fermi level position, intentional doping with transition metal ions, and segregation phenomena.

The dense graphite used in construction of the crucible and crucible lid was purchased from Graphite DieMold (Durham, CT) while the susceptor, support rod, and ring was purchased from UCAR (Parma, OH, graphite-type DT 223). After machining, all graphite elements underwent a proprietary purification procedure, including annealing at 2000 °C in an atmosphere containing chlorine. The typical impurity concentrations in both materials obtained by Glow Discharge Mass Spectroscopy (GDMS) is shown in Tables 1 and 2.

Table 1. GDMS Analysis Data of UCAR DT 223 Graphite Material.

Element	Concentration (ppm) GDMS	Concentration (ppm) ICP	Concentration (ppm) DC-Arc
Al	<0.3 (1.3 max)	<0.1 (0.14 max)	<0.2 (0.2 max)
Sb	<0.1	N/m	<0.2
As	<0.1	N/m	<0.2
Bi	<0.1	N/m	<0.2
B	<0.3 (0.4 max)	N/m	<0.2 (0.2 max)
Ca	<0.1 (0.15 max)	<0.1	<0.2 (
Cr	<0.1	<0.1	<0.2
Co	<0.1 (0.28 max)	N/m	N/m
Cu	<0.1	<0.1	<0.2
Fe	<0.2 (0.35 max)	<0.2 (0.5 max)	<0.2 (0.7 max)
Mg	<0.1	<0.1	<0.2 (0.2 max)
Mn	<0.1	<0.1	N/m
Mo	<0.1	<0.1	N/m
Ni	<0.1 (0.17 max)	<0.1 (0.32 max)	<0.2 (0.9 max)
K	<0.1	<0.1	<0.2
Si	<0.5	<0.1	<0.2
Sr	<0.1	<0.1	N/m
Sn	<0.1	<0.1	N/m
Ti	<0.1	<0.1	<0.2
W	<0.1 (0.4 max)	N/m	N/m
V	<0.1	<0.1 (0.11 max)	<0.2 (0.3 max)
Zn	<0.1	<0.1	<0.2 (0.3 max)
Zr	<0.1	<0.1	N/m

Table 2. GDMS Analysis Data of Graphite DieMold CG 23 Graphite Material.

Element	Concentration (ppm)	Element	Concentration (ppm)
Al	0.2	Ba	0.01
B	0.2	Ca	0.15
Cu	0.02	Cr	0.2
Co	0.05	Fe	0.2
Pb	0.01	Li	0.005
Mg	0.005	Mn	0.02
Mo	0.02	Ni	0.02
K	0.1	P	0.1
Na	0.15	Sr	0.015
Th	0.005	Sn	0.015
Ti	0.2	W	0.15
U	0.005	V	0.05
Zn	0.01	Zr	0.05

The purification procedure used by UCAR reduced concentrations of all metals to the level below 0.2 ppm, with the highest concentrations detected due to iron, vanadium, nickel, and aluminum. Aluminum and boron concentrations (both serve as shallow acceptors in SiC) added up to 0.5 ppm. Data on Graphite DieMold material are essentially identical, with the exception of lower vanadium concentrations. Every growth run was performed in a new crucible and employed a new crucible lid. The susceptor and graphite insulation were reused in all growth runs. The lifetime of both elements exceeds 30 runs, and it was assumed that there was no change in the chemical or structural properties of either element after the first 5 growth runs.

Another likely source of residual impurities was the SiC charge material. Two different grades of charge material have been purchased from commercial vendors. H. C. Starck (Selb, Germany) material was produced by Chemical Vapor Deposition (CVD) and had a form of a fine powder with the grain size of about 7 μm in diameter. The acceptor concentration was in a ppm range (boron 3 ppm, aluminum 1 ppm) with several transition metal impurities also above 1 ppm (titanium, chromium, and iron). All GDMS data are listed in Table 3. GDMS analysis performed by Shiva Technologies does not cover nitrogen. The characteristic green coloration of the charge material would indicate a substantial nitrogen concentration.

Table 3. GDMS Analysis Data of SiC Charge Powder Purchased from H. C. Starck.

	Concentration	Element	Concentration
Li	<0.05	Ag	<0.05
Be	<0.01	Cd	<0.5
B	3.0	In	Binder
C	Matrix	Sn	0.30
F	<0.5	Sb	<0.05
Na	2.9	Te	<0.05
Mg	0.45	I	<0.05
Al	1.0	Cs	<0.01
Si	Matrix	Ba	<0.05
P	0.25	La	0.02
S	2.0	Ce	<0.05
Cl	1.0	Pr	<0.05
K	0.03	Nd	<0.05
Ca	1.6	Sm	<0.05
Sc	<0.05	Eu	<0.05
Ti	1.1	Gd	<0.05
V	<0.01	Tb	<0.05
Cr	1.3	Dy	<0.05
Mn	0.04	Ho	<0.05
Fe	1.4	Er	<0.05
Co	<0.05	Tm	<0.05
Ni	0.15	Yb	<0.05
Cu	0.25	Lu	<0.05
Zn	0.5	Hf	<0.05
Ga	<0.05	Ta	<1.0
Ge	<0.05	W	0.20
As	<0.05	RE	<0.05
SE	<0.1	Os	<0.05
Br	<0.1	Ir	<0.01
Rb	<0.01	Pt	<0.05
Sr	<0.01	Au	<0.5
Y	<0.05	Hg	<0.1
Zr	0.10	Tl	<0.01
Nb	<0.05	Pb	<0.05
Mo	<0.05	Bi	<0.05
Ru	<0.05	Th	<0.01
Rh	<0.01	U	<0.01
Pd	<0.05		

Table 4. GDMS Analysis Data on SiC Charge Powder Purchased from Advanced Materials

Element	Concentration	Element	Concentration
Li	<0.001	Be	<0.005
B	0.84	Na	<0.01
Mg	<0.01	Al	0.025
P	0.01	S	0.03
K	<0.05	Ca	<0.05
Sc	<0.001	Ti	<0.001
V	0.13	Cr	<0.1
Mn	<0.01	Fe	0.1
Co	0.02	Ni	0.61
Cu	<0.05	Zn	<0.05
Ga	<0.05	Ge	<0.05
As	<0.01	Se	<0.05
Br	<0.05	Rb	<0.01
Sr	<0.005	Y	<0.01
Zr	<0.01	Nb	<0.01
Nb	<0.01	Mo	<0.05
Ru	<0.01	Rh	<0.005
Pd	<0.01	Ag	<0.01
In	<0.01	Sn	<0.05
Sb	<0.01	Te	<0.01
I	<0.005	Cs	<0.005
Ba	<0.005	La	<0.005
Ce	<0.005	Pr	<0.005
Nd	<0.005	Sm	<0.005
Eu	<0.005	Gd	<0.005
Tb	<0.005	Dy	<0.005
Ho	<0.005	Er	<0.005
Tm	<0.005	Yb	<0.005
Lu	<0.005	Hf	<0.005
Ta	5	W	<0.01
Re	<0.01	Os	<0.01
Ir	<0.005	Pt	<0.01
Au	<0.05	Hg	<0.05
Hg	<0.05	Tl	<0.005
Pb	<0.005	Bi	<0.005
Th	<0.001	U	<0.001

Charge material purchased from Advanced Materials (Woburn, MA) was also produced by the CVD method but was originally in a form of thick solid sheets. The material was broken up into chunks with typical size of 5 mm. The analysis data given below pertain to the original solid rather than average purity of chunks (Table 4). The acceptor densities B = 0.8 ppm, and Al =0.03 ppm) are significantly lower than that of Starck material. It is likely the consequence of the fact that the Starck CVD reactor is used for production of other ceramic powders such as boron nitride. Transition metal concentrations are also lower (Fe = 0.1 ppm, Ni = 0.6 ppm, and V = 0.1 ppm). However, the material can be contaminated in the milling process and the resulting metal content is likely higher than that given in Table 4. The scattered data indicate that contamination introduced during milling process vary widely from batch to batch.

In addition to controlling solid contaminants present in the hot zone materials, one needs to control the amount of gases adsorbed on the graphite furniture. It is an important aspect of the pregrowth procedures, as the very large surface area of porous graphite does adsorb very significant amounts of nitrogen, water, and oxygen. Clearly, all of these elements (nitrogen, hydrogen, and oxygen) can play a crucial role in electrical properties. The removal of gases was accomplished by extensive annealing of the hot zone and charge material. After loading, the reactor was evacuated using a rotary vacuum pump to vacuum better than 10^{-3} torr and backfilled with ultra-high-purity (UHP) argon (99.9999 percent). The procedure was repeated four times. This was followed by evacuation with a turbo-molecular pump to vacuum better than 10^{-6} torr, which took approximately 3 hours. After reaching this level the power for the heating inverter was turned on and slowly increased while monitoring the pressure in the chamber and temperature. With increasing temperature, the gas desorption rate increases exponentially, increasing, as a result, the background pressure in a chamber. The rate of heating was adjusted in order to keep the residual pressure below 10^{-4} torr. After reaching 1200 °C, the power was stabilized and the chamber was evacuated to pressure below 10^{-6} torr. Typically the system was left under vacuum at 1200 °C overnight.

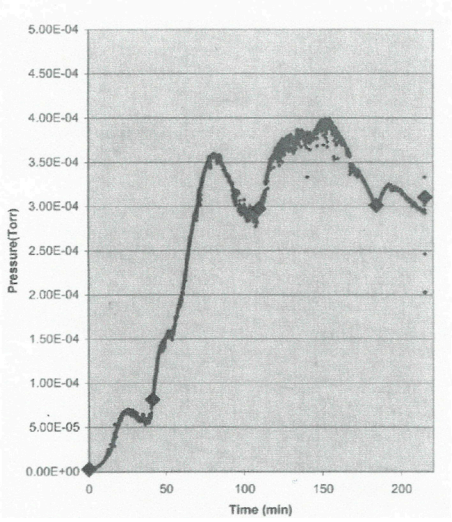

Figure 3. Typical outgasing sequence of hot zone elements/seed/charge material.

2.3 Crystals Used in Analysis.

The five boules analyzed in this study are shown in Figures 4 through 8 followed by the brief description of features that are characteristic of each growth run. Crystal 1 is shown in Figure 4. The charge material used was obtained from Advanced Materials with no intentional dopants added to the crucible. The boule shows a relatively large central facet with well-defined steps propagating radially toward the boule periphery. The seed was attached to the crucible lid using molten sucrose. The total height of the boule was about 11 mm. As for all of the other crystals in this series, the boule was sliced, with three wafers used for analysis from the locations shown in Figure 4.

(a)

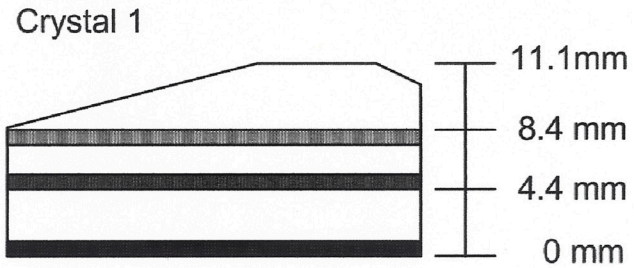

(b)

Figure 4. Photograph of crystal 1 still attached to the crucible lid (a) and schematic drawing indicating positions of wafers used in analysis (b).

Crystal 2 was grown using a Starck charge with the seed wafer mounted using a retaining ring. The back surface of the seed was protected with a layer of graphitized photoresist. Remains of the seed wafer edges are still visible around the crystal periphery. The protection layer partially delaminated during growth, resulting in the formation of hexagonal void defects. All of these defects remained within or close to original seed and none were present in the analyzed wafers. Since the void motion amounts to regrowth of the solid with possible incorporation of impurities characteristic of later stages of growth,

it is important to avoid areas though which voids moved through. The change of the charge material compared to boule 1 resulted in a slightly lower overall growth rate.

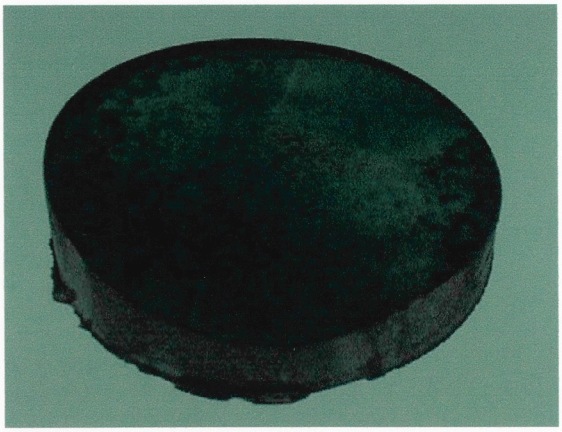

(a)

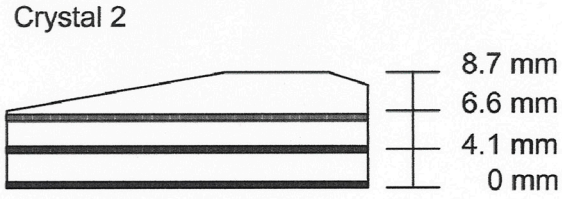

(b)

Figure 5. Optical image of the crystal 2 (a) with the schematic representation of wafer locations (b).

Boule 3 was grown using Advanced Materials charge, with an additional surface cleaning step consisting of etching in hot H_2SO_4:H_2O_2 followed by the deionized (DI) water rinse and high temperature (1200 °C) annealing step. No intentional dopants have been added. The growth rate was slightly higher than in the case of boule 1, possibly due to the retaining ring used for seed attachment, resulting in lower crystal temperature and higher gradient. Higher temperature gradient also was reflected in a change of shape of the growth interface remaining convex in the center of the boule but becoming concave toward the crystal periphery. The growth surface shows the presence of macroscopic defects appearing as narrow slits with planes determined by [0001] and <1-100> directions. The slits extended about 4 mm from the top surface into the volume of the boule. Care was taken to select Hall samples from the unaffected part of the boule.

(a)

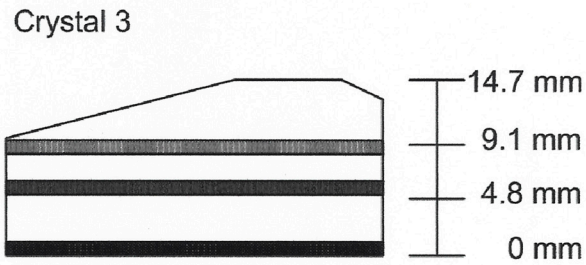

(b)

Figure 6. Optical image of the boule 3 (a) and schematic diagram of wafer locations (b).

Crystal 4 was grown using a prepurified Advanced Materials source using the same seed attachment as boule 3. In addition, 0.3 grams of pure iron was added to the charge material. Assuming a 0.1 segregation coefficient, this amount of dopant should result in concentrations in the 10^{17} cm^{-3} range. This is close to the reported solid solubility limits of transition metal ions in SiC at typical PVT growth temperatures. The growth surface was covered by macrosteps, which is typical of low growth rates at later stages of growth and carbon-rich ambient. A possible reason for the lower growth rate was the increased loss of vapor species from the growth crucible. Since the vapor is always silicon rich, this led to a carbon-rich charge at the end of the growth run.

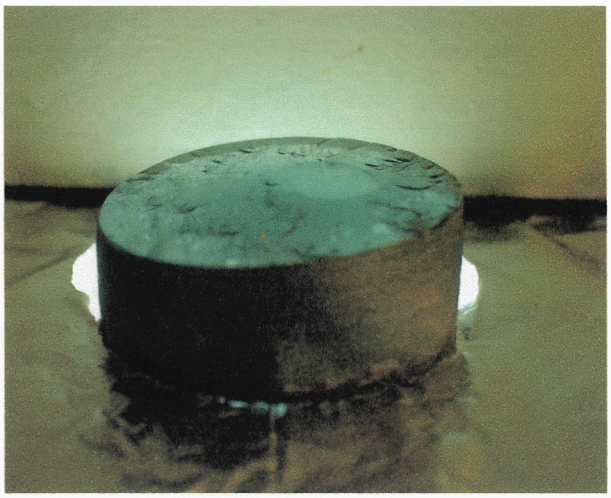

(a)

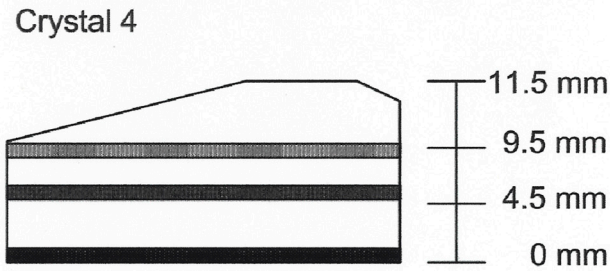

(b)

Figure 7. Optical image of boule 4 (a) and schematic diagram of wafer locations (b)

Boule 5 is shown in Figure 8 with the carbon protection layer removed. Light could easily penetrate the entire thickness of the boule as was characteristic of all other boules (not obvious in illumination conditions used for photographs). The coloration was a light shade of grayish-blue typical of slightly p-type 6H-SiC. In transmission, one could see several deep slits around the periphery of the boule, similar to those observed in boule 3. It is interesting to note that the growth rate for both boule 3 and 5 was the highest of all five runs, indicating the correlation between growth rate and slit formation. The charge material used was obtained from Advanced Materials and an additional 0.4 grams of metallic cobalt was added to the charge.

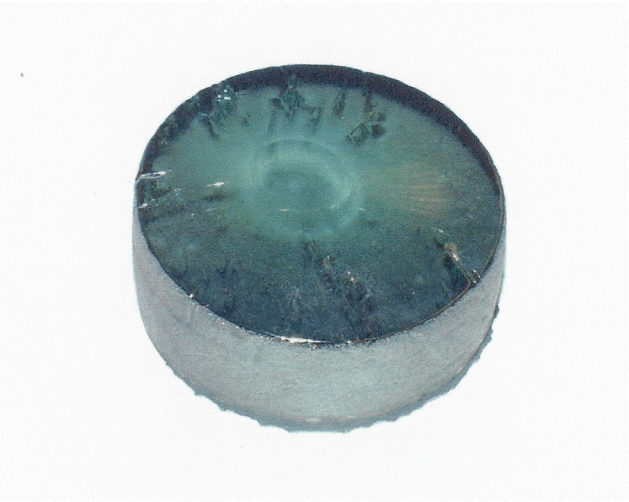

(a)

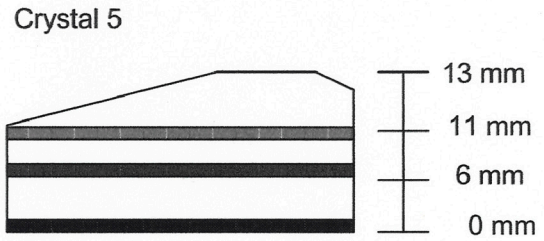

(b)

Figure 8. Optical image of the boule 5 (a) and schematic diagram of wafer locations (b).

Three wafers were cut from each one of the boules analyzed in this project at the locations indicated by part (b) of each drawing. Both surfaces were subsequently lapped with boron carbide abrasive, followed by mechanical polishing using different grades of diamond paste. The final finish was obtained with 1-μm-grit diamond compound.

3. Chemical Analysis and Segregation of Impurities.

3.1 Methodology

Two complementary methods have been used for chemical analysis of the grown wafers. The GDMS performed by Shiva Technologies (Syracuse, NY) was used to monitor all impurities, with the exception of nitrogen. The samples were prepared in a form of a square piece of the wafer with the lateral size of 7 mm. Possible surface contaminants have been removed by in situ sputtering.

Since GDMS is not capable of detecting nitrogen in concentrations lower than 10^{20} cm^{-3}, the concentrations of this impurity were monitored with secondary ion mass spectroscopy (SIMIS) performed by Charles Evans and Associates.

3.2 Major impurity species and segregation

3.2.1 Acceptors

The dominant acceptor specie in SiC grown in this project was boron. For all samples analyzed, the boron concentration was in the $5x10^{16}$-$5x10^{17}$ cm^{-3} range. The results are presented in a graphical form in Figure 9. It is apparent from these data that the crystal with highest overall boron concentration was grown using the H. C. Starck charge material. Typical concentrations of boron in crystals grown using Advanced Materials charge had boron concentrations lower by about a factor five. The only exception was crystal 3, which had only slightly lower boron content than that of crystal 2. The correlation of charge material with boron content in crystals leads us to believe that boron concentrations above $2x10^{17}$ cm^{-3} originate from charge.

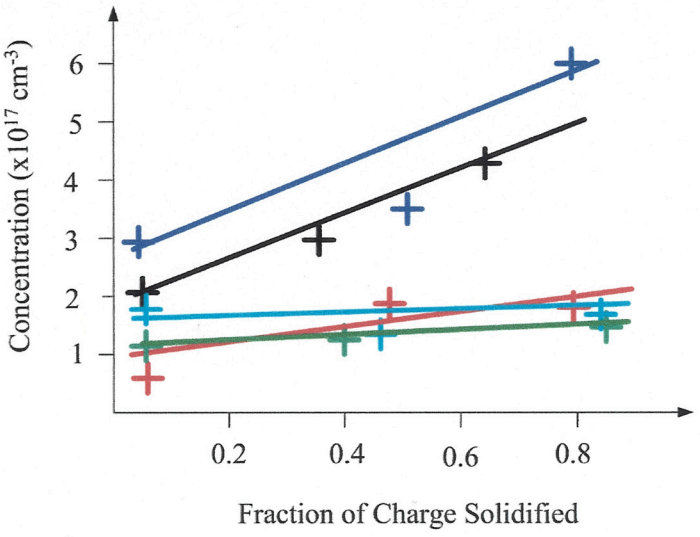

Figure 9 Boron concentration as a function of fraction of the charge solidified

Figure Note: blue line and points: boule 1, black: boule 3, light blue: boule 1, red: boule 4, and green: boule 5).

In all SiC boules analyzed, boron concentration increased from seed toward the tail of the boule. The segregation coefficient varied from 0.95 to 0.7, with the lowest values obtained on crystals with the highest boron concentration. In fact, all five boules can be separated into two groups: one containing boules 1, 4, and 5, which showed almost constant boron concentration (all boules were grown from Advanced Materials charge), and boule 2, which demonstrated significant boron variation. The origin of this difference is not clear at present.

The second significant acceptor type impurity in our boules was aluminum. Its concentrations were approximately an order of magnitude lower than that of boron. As in the case of boron, the crystal grown using Starck material had the highest concentration of aluminum, which in the tail part of the boule was about an order of magnitude higher than that of boules grown with Advanced Materials charge. Aluminum segregated toward the end of the boule in two crystals (1 and 2), and either remained constant or slightly decreased in the remaining three boules. Lack of consistent behavior does not allow to reach conclusions as to the source and mechanism of incorporation of aluminum.

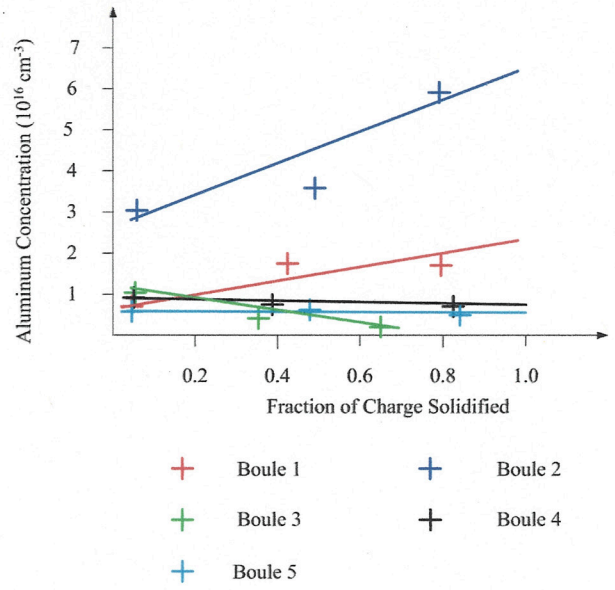

Figure 10. Aluminum concentration as a function of fraction of charge solidified

3.2.2 Nitrogen

Since the nitrogen has to be analyzed separately from other impurities and the cost is $350 per sample, we limited the analysis to only one set of three wafers from one boule due to budgetary constraints. The results are presented in Figure 11. The concentration was relatively high and remained in the 1-2x10^{17} cm^{-3} range throughout the boule. It is somewhat unexpected that the nitrogen content did not drop off more rapidly with the

growth time as the most obvious source of the contamination, namely gas adsorbed in the porous graphite, should desorb relatively fast at high temperatures. This points toward the source powder as an alternative source. The mass spectrometry data on main shallow impurities do not agree very well with results of Hall effect measurements. The correlations are discussed in the following section.

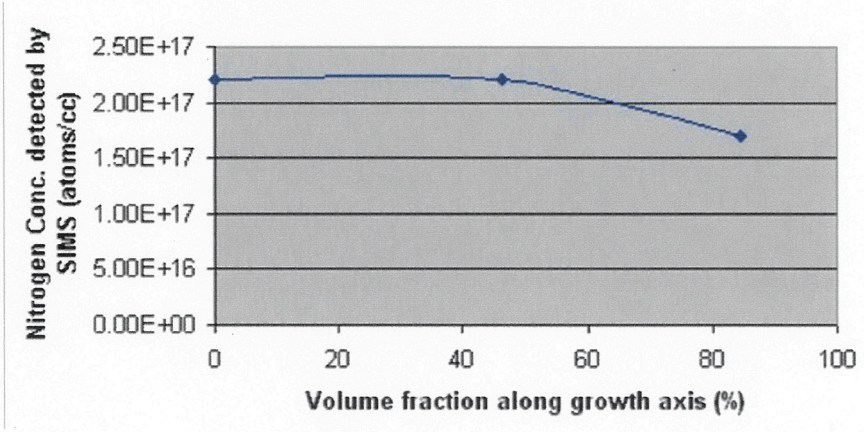

Figure 11 Nitrogen concentration monitored by SIMS in boule 5 as function of fraction of the charge solidified

3.2.3 Transition Metals

Vanadium, chromium, manganese, cobalt, and nickel were below their respective GDMS detection limits in all wafers from all boules (N_V=1.5x10^{15} cm^{-3}, N_{Cr}=3x10^{15} cm^{-3}, N_{Mn}=3x10^{14} cm^{-3}, and N_{Ni}=3x10^{14} cm^{-3}). All others were close to the detection limits and are listed in Table 5.

Table 5 Concentrations of titanium in wafers (in 10^{15} cm^{-3})

Titanium	Seed	Middle	Tail
Boule 1	<0.3	<0.3	<0.3
Boule 2	<0.3	<0.3	0.3
Boule 3	0.6	0.18	0.3
Boule 4	<0.3	<0.3	<0.3
Boule 5	<0.3	<0.3	<0.3

Table 6 Concentrations of iron in wafers (in 10^{15} cm^{-3})

Iron	Seed	Middle	Tail
Boule 1	1.7	2.8	2.8
Boule 2	11.2	2.4	2.4
Boule 3	<0.3	1.4	0.3
Boule 4	<0.3	1.7	2.4
Boule 5	1.0	1.4	1.7

Table 7 Concentrations of copper in wafers (in 10^{15} cm^{-3})

Copper	Seed	Middle	Tail
Boule 1	<0.05	<0.05	<0.05
Boule 2	0.8	0.2	2
Boule 3	0.2	0.4	0.06
Boule 4	<0.05	<0.05	<0.05
Boule 5	<0.05	<0.05	<0.05

The concentrations of all transition metals are too close to their respective detection limits to allow for meaningful interpretation. It is important to note that both intentional dopants (iron and cobalt) failed to incorporate at concentrations above detection or background values.

4. Transport Measurements and Compensation in PVT 6H-SiC Boules (Hall Effect Measurements).

The room temperature carrier concentrations determined from Hall effect measurements are presented in Table 8. There are several common features that apply to all of the boules. The first wafer from each boule was n-type with the Fermi level pinned close to the conduction band. The carrier concentrations varied by several orders of magnitude, in some cases, well below the impurity concentrations. The mid wafers were either n-type with electron concentration lower than that of seed wafer or high-resistivity p-type. The tail of each boule was p-type. This general trend of Fermi level monotonically dropping down with the increase of the mole fraction solidified agrees with the major trends in behavior of impurities, namely, the decrease of nitrogen content along the growth axis from seed to tail, and increase of boron content.

Table 8 Room temperature carrier concentration data

Crystal	Seed	Mid	Tail
Boule 1	n, $7x10^{16}$ cm^{-3}	n, $3x10^{9}$ cm^{-3}	p, $3x10^{9}$ cm^{-3}
Boule 2	n, $3.4x10^{18}$ cm^{-3}	n, $5.4x10^{17}$ cm^{-3}	p, $1.1x10^{16}$ cm^{-3}
Boule 3	n, $3x10^{16}$ cm^{-3}	n, $5x10^{14}$ cm^{-3}	p, $3.3x10^{14}$ cm^{-3}
Boule 4	n, $3x10^{13}$ cm^{-3}	p, $1x10^{12}$ cm^{-3}	p, $2x10^{12}$ cm^{-3}
Boule 5	n, ND	n, ND	p, $2x10^{12}$ cm^{-3}

The boule with highest free electron concentration was boule 2 grown from the Starck charge. The electron concentration was almost two orders of magnitude higher than that of the next highest. First to grow part boule exhibited high n-type conductivity turning p-type only in the tail section. This behavior is a clear indication that the charge powder was the source of nitrogen contamination.

Boules 1 and 2 grown from the as-received and treated Advanced Materials charge both turned n-type in the first wafer with electron concentrations in mid 10^{16} cm^{-3}. It is interesting to note that both boules intentionally doped with transition metals had electron

concentrations at least three orders of magnitude lower. The impurities (iron and cobalt) have been predicted to act as acceptors in the 6H-SiC, and this decrease of electron concentration seems to be in agreement with this prediction. The tail wafer from boule 2 had highest free hole concentration (low 10^{16} cm^{-3}) at room temperature. This is in agreement with the mass spectroscopy data. Below are the results of high-temperature Hall data obtained on middle and/or tail wafers from all boules. In all cases, Hall voltage was too small to measure reliably and, as a consequence, the determination of mobility and carrier concentrations was not possible. The data are limited to resistivity and, in some cases, only temperature range above 200 °C. At low temperatures, the voltage drop across metalsemiconductor contacts was too high to produce reliable data.

Both the middle and tail wafers from boule 1 were highly resistivitive with resistivities in excess 10^6 ohm cm. Both plots show an anomalous behavior in the low temperature range possibly affected by contacts or surface conductivities. The bulk resistivity extrapolated from high-temperature data was 10^{12} and 10^9 ohm cm for the middle and tail wafers, respectively.

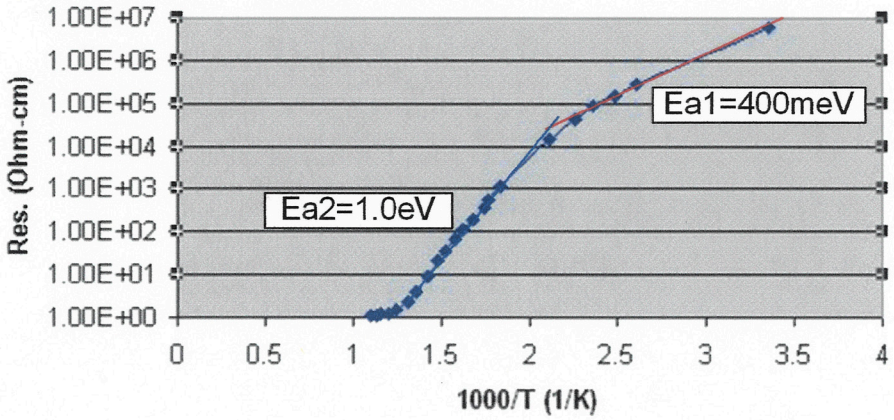

Figure 12 Resistivity versus T^{-1} obtained on the middle wafer from boule 1

The linear approximation of the high temperature range gives an activation energy of 1 eV. The sign of the Hall voltage indicates an n-type material, meaning that the Fermi level is pinned at 1 eV below conduction band. Such a level was previously reported by Mitchel et al. [1] and Mueller et al. [2] in vanadium-free, semi-insulating 4H SiC. One of the possible assignments for such level is a defect associated with oxygen presence in the material. The data for the tail wafer from the same boule are shown in Figure 13.

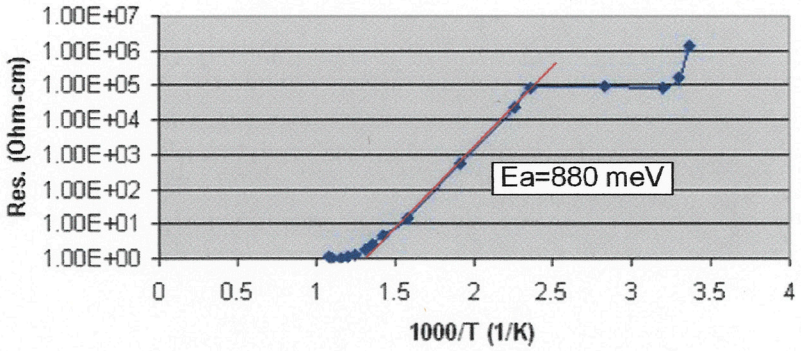

Figure 13 Resistivity versus T^{-1} obtained on the tail wafer from boule 1.

The conductivity was of p-type character with an activation energy of 0.88 eV. This corresponds to approximately a 1 eV drop in Fermi energy position between middle and tail wafers in line with results on other boules. To our knowledge, a level positioned approximately 0.9 eV above the valence band has not been reported. Boule 1 exhibited a remarkably large portion with high resistivities.

Boule 2 had the highest impurity count of all boules, with the conductivity of the seed and middle wafers dominated by a shallow nitrogen donor. The tail wafer was definitely p-type, with the activation energy of 0.3 eV (Figure 14).

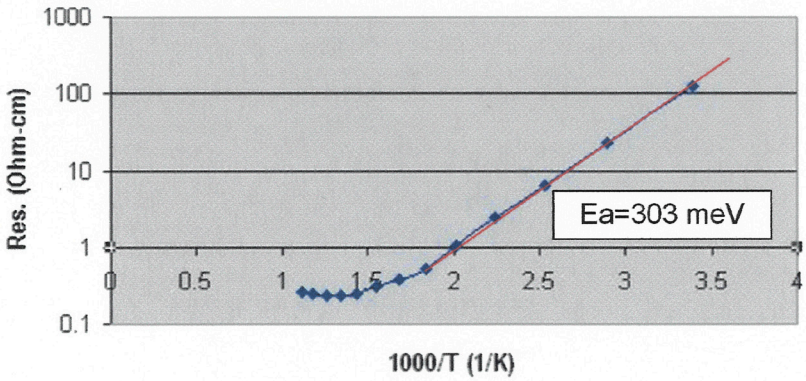

Figure 14 Resistivity versus T^{-1} obtained on the tail wafer from boule 2.

Such activation energy has been observed many times and is well documented to be due to a shallow boron acceptor [3]. This is in good agreement with the high boron content detected by GDMS. Tail wafers from boules 3 and 4 also show activation energies characteristic of boron acceptors (Figures 15 and 16).

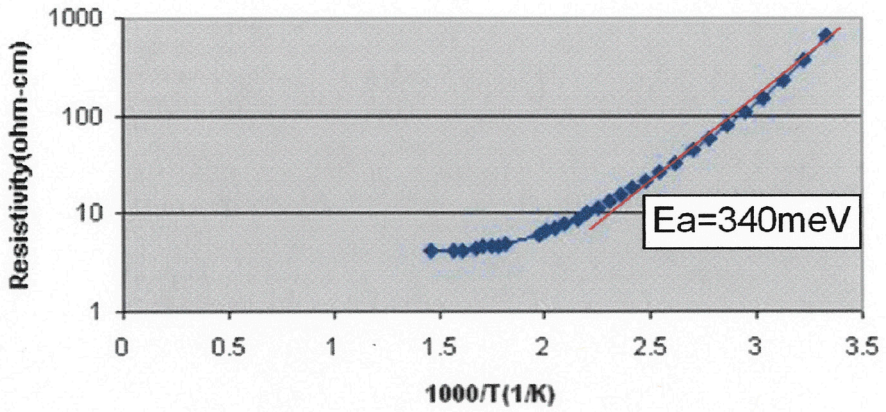

Figure 15. Resistivity versus T^{-1} obtained on the tail wafer from boule 3.

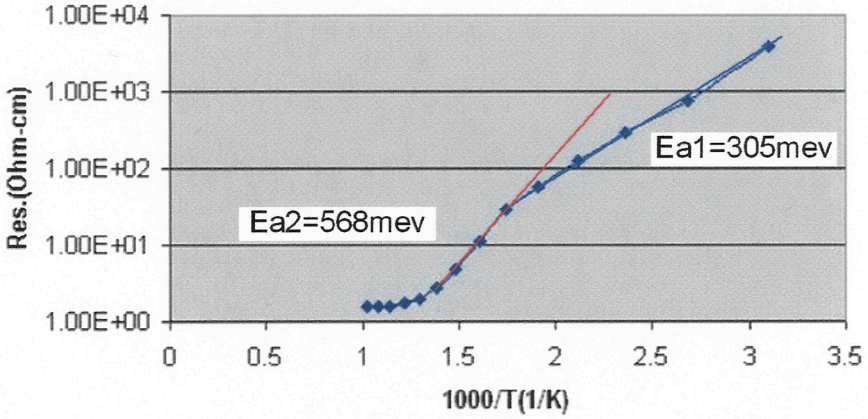

Figure 16. Resistivity versus T^{-1} obtained on the tail wafer from boule 4.

Both boule 4 and 5 have a higher activation energy component visible at high temperatures. The activation energies are 0.57 eV and 0,48 eV, respectively. Both of them fall in the region that have been associated with a deep boron state. Other than lower electron concentrations in the seed part of both boules, the crystals doped with cobalt and iron did not show any sign of transition metal activity.

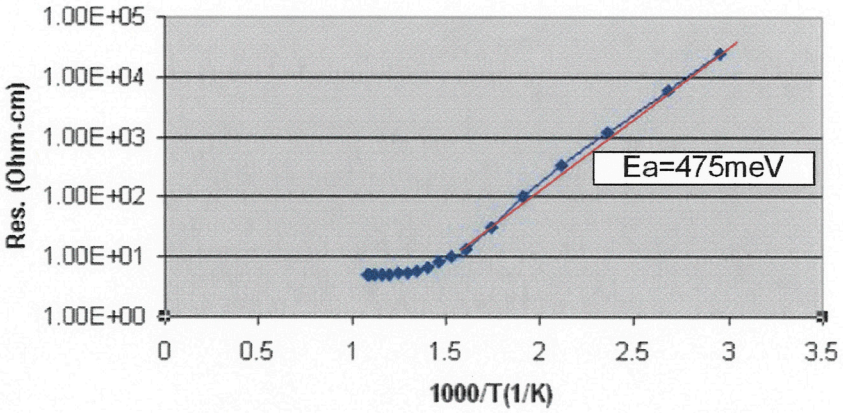

Figure 17. Resistivity versus T^{-1} obtained on the tail wafer from boule 5.

5. Summary

SiC boules have been grown by PVT method and analyzed using GDMS and SIMS and transport methods. The dominant impurities are nitrogen in the seed part of the boules and boron in the tail part. Nitrogen concentrations decrease toward the tail, while that of boron and aluminum increases. The major source of these contaminants was the commercial charge material. For further studies of impurities and deep levels in this material, it is critical to eliminate this contamination source by synthesizing a pure charge. Since none of the current commercial sources is acceptable for growth of semi-insulating SiC crystals, it would be of great benefit for the SiC industry to develop a new grade of pure SiC charge. The Fermi level in all crystals grown during this project started at being pinned to a nitrogen donor level in the seed end of the boule and dropped to the shallow boron acceptor level at the tail end. The middle part exhibited either a narrow or wide band of high resistivity material, depending primarily on the impurity content and segregation. In general, lower boron and nitrogen concentrations resulted in a larger percentage of the boule being high resistivity. The transition metals segregate quite severely and have a low incorporation coefficient in 6H-SiC. The concentration of intentional dopants (iron and cobalt) were below mass spectroscopy detection limit. The intentional doping correlated with lower free electron concentration in the seed part of the doped boules, which is in agreement with their expected acceptor-like behavior.

6. References

1. W.C. Mitchel, A. Saxler, R. Perrin, J. Goldstein, S.R. Smith, A.O. Evwaraye, J.S. Solomon, M. Brady, V. Tsvetskov, and C. H. Carter, *Mater. Sci. Forum*, **338-342** 21, 2000.
2. S.G. Mueller, M. Brady, B. Brixius, G. Fechko, R.C. Glass, F.D. Henshall, H.M. Hobgood, J.R. Jenny, R. Leonard, D. Malta, A. Powell, V.F. Tsvetskov, and C. H. Carter, *Mater. Sci. Forum*, in print, 2002.
3. J.R. Jenny, M. Skowronski, W.C. Mitchel, H.M. Hobgood, R.C. Glass, G. Augustine, and R.H. Hopkins, *J. Appl. Phys.*, **79** 2326, 1996.

List of Acronyms

CBCF	carbon-bonded carbon fiber
CVD	chemical vapor deposition
DI	deionized
GDMS	glow discharge mass spectroscopy
PVT	physical vapor transport
RF	radio frequency
SiC	silicon carbide
SIMS	secondary ion mass spectroscopy